


Article

The Impact of a Check Dam on Groundwater Recharge and Sedimentation in an Ephemeral Stream

Hakan Djuma ^{1,*} , Adriana Bruggeman ¹, Corrado Camera ^{1,2}, Marinos Eliades ¹ and Konstantinos Kostarelos ³

¹ Energy, Environment and Water Research Centre, The Cyprus Institute, 2121 Aglantzia, Nicosia, Cyprus; a.bruggeman@cyi.ac.cy (A.B.); c.camera@cyi.ac.cy (C.C.); m.eliades@cyi.ac.cy (M.E.)

² Dipartimento di Scienze della Terra “A. Desio”, Università degli Studi di Milano, 20133 Milan, Italy

³ UH Energy Research Park, University of Houston, Houston, TX 77204-0945, USA; kkostare@Central.UH.EDU

* Correspondence: h.djuma@cyi.ac.cy; Tel.: +357-22-208607

Received: 18 September 2017; Accepted: 19 October 2017; Published: 24 October 2017

Abstract: Despite the widespread presence of groundwater recharge check dams, there are few studies that quantify their functionality. The objectives of this study are (i) to assess groundwater recharge in an ephemeral river with and without a check dam and (ii) to assess sediment build-up in the check-dam reservoir. Field campaigns were carried out to measure water flow, water depth, and check-dam topography to establish water volume, evaporation, outflow, and recharge relations, as well as sediment build-up. To quantify the groundwater recharge, a water-balance approach was applied at two locations: at the check dam reservoir area and at an 11 km long natural stretch of the river upstream. Prediction intervals were computed to assess the uncertainties of the results. During the four years of operation, the check dam (storage capacity of 25,000 m³) recharged the aquifer with an average of 3.1 million m³ of the 10.4 million m³ year⁻¹ of streamflow (30%). The lower and upper uncertainty limits of the check dam recharge were 0.1 and 9.6 million m³ year⁻¹, respectively. Recharge from the upstream stretch was 1.5 million m³ year⁻¹. These results indicate that check dams are valuable structures for increasing groundwater resources in semi-arid regions.

Keywords: water balance model; discharge measurement; sedimentation; infiltration; managed aquifer recharge; estimation errors; Cyprus; Mediterranean Island

1. Introduction

Groundwater is an important source of water supply in semi-arid regions because it is protected from high evaporation rates that affect surface water bodies. The sustainability of groundwater bodies is therefore very important, and induced groundwater recharge is one of the main methods for increasing the sustainable yield of a groundwater body [1–3]. Especially under climate change conditions, managed aquifer recharge systems could be more effective than increasing surface reservoir capacities [4] and could also be the most economically and socially feasible solution for the integrated management of water resources [5].

A recharge check dam is a barrier that is placed across a river or channel to slow the movement of water, encouraging groundwater recharge. Several authors studied the groundwater recharge efficiency of check dams. Martin-Rosales et al. [6] quantified recharge by estimating the infiltration capacity of the reservoir bed of existing check dams by infiltrometer tests in south-eastern Spain. Infiltrometer tests could also be performed to test the infiltration of different geological units [7]. Alderwish [8] quantified groundwater recharge from three projected check dams in Yemen. The author compared a simple water balance model based on average measured saturated hydraulic conductivity with a two dimensional recharge expression, based on Darcy’s law. He found that the total calculated recharge

rate over a 20 year period (2007 to 2026) using the Darcian approach was close to that calculated by the water balance method. He concluded that a simple water balance approach can provide acceptable results for the estimation of induced recharge when the scarcity of site-specific data limits the use of sophisticated analysis techniques. Racz et al. [9] found great spatial and temporal variations in pond infiltration rates, even in a single aquifer recharge reservoir. They noted that locations with the most rapid infiltration shifted laterally during the aquifer recharge event. However, few water balance studies at a single check dam with field data have been presented in the literature [9,10], and none presented associated uncertainties of their estimates.

Recharge behind the check dam is affected not only by its location [11] but also by the build-up of sediment in its reservoir. This sediment build-up is a result of riverbank erosion or erosion in the upstream watershed area, which is affected by land use, climate, topography, and soils [12–18]. Sediment build-up and infiltration at check dams are generally studied separately, although the former can increase the uncertainty in the estimates of the latter, especially for water balance calculations.

The objectives of this study were (i) to assess groundwater recharge in an ephemeral river with and without check dam and (ii) to assess the average annual sedimentation rate at the check dam during a four year period (2011 to 2015). The study was conducted on a check dam in the semi-arid island of Cyprus. Field campaigns were carried out to measure water flow, water depth, and check dam topography in order to establish check dam water volume, evaporation, outflow, and recharge relations. A water balance model was developed according to these relations and applied at two locations for the quantification of the groundwater recharge. The first location is at the check dam reservoir, while the second is along a natural stretch of river bed upstream of the check dam reservoir. Uncertainties of the estimates are reported in the form of prediction intervals.

2. Materials and Methods

2.1. Study Area

This study was conducted in the Peristerona Watershed in Cyprus. The Peristerona River has an ephemeral water flow and is located on the north-eastern hill slope of the Troodos Mountains (Figure 1). In its upstream part, the elevation ranges between 1540 and 900 m, with a mean local slope higher than 40% and a mean average precipitation (1980 to 2010) of 750 mm [19]. The geology of this area is dominated by intrusive rocks (sheeted dykes-Diabase), with smaller areas of cumulate rocks (gabbro and plagiogranites), of the Troodos ophiolitic sequence [20,21]. Upstream, the land is covered mostly with sclerophyllous forests and mountain agriculture on terraces retained by dry-stone walls. Many of these terraces are abandoned with collapsed walls, and options for rehabilitation are being investigated [22]. The midstream area ranges between 900 and 500 m above sea level (a.s.l.). The geological formations consist of intrusive rocks of the basal group (over 50% dykes with screens of pillow lavas) and are mainly covered by pine forests, with an annual precipitation of 405 mm. The foothills of the Troodos Mountains are formed by pillow lavas (olivine, pyroxene, and phyrlic lavas) and outcrops of sedimentary formations (hydrothermal and deep water sediments: umbers, shales, and mudstones) with occasional pockets of highly saline groundwater. The elevation ranges between 500 to 300 m a.s.l., with mean local slope of 20% and 360 mm annual precipitation. Within the downstream Mesaoria plain, the watershed narrows, and the mean local slope is lower than 8%, with an average precipitation of 270 mm. The geology mainly consists of sedimentary formations (mostly alluvium-colluvium: sands, silts, clays, and gravel) from the Pleistocene and the Holocene, which form a shallow unconfined groundwater system in connection with the riverbed [23]. The Peristerona River recharges the alluvium and the sedimentary Central and Western Mesaoria Aquifer (Figure 1), which is the largest and most important groundwater reservoir in Cyprus [24]. Karydas et al. [25], who applied the empirical erosion model G2 to the Republic of Cyprus, found soil loss rates exceeding 20 tons hectare⁻¹ in the Peristerona watershed.

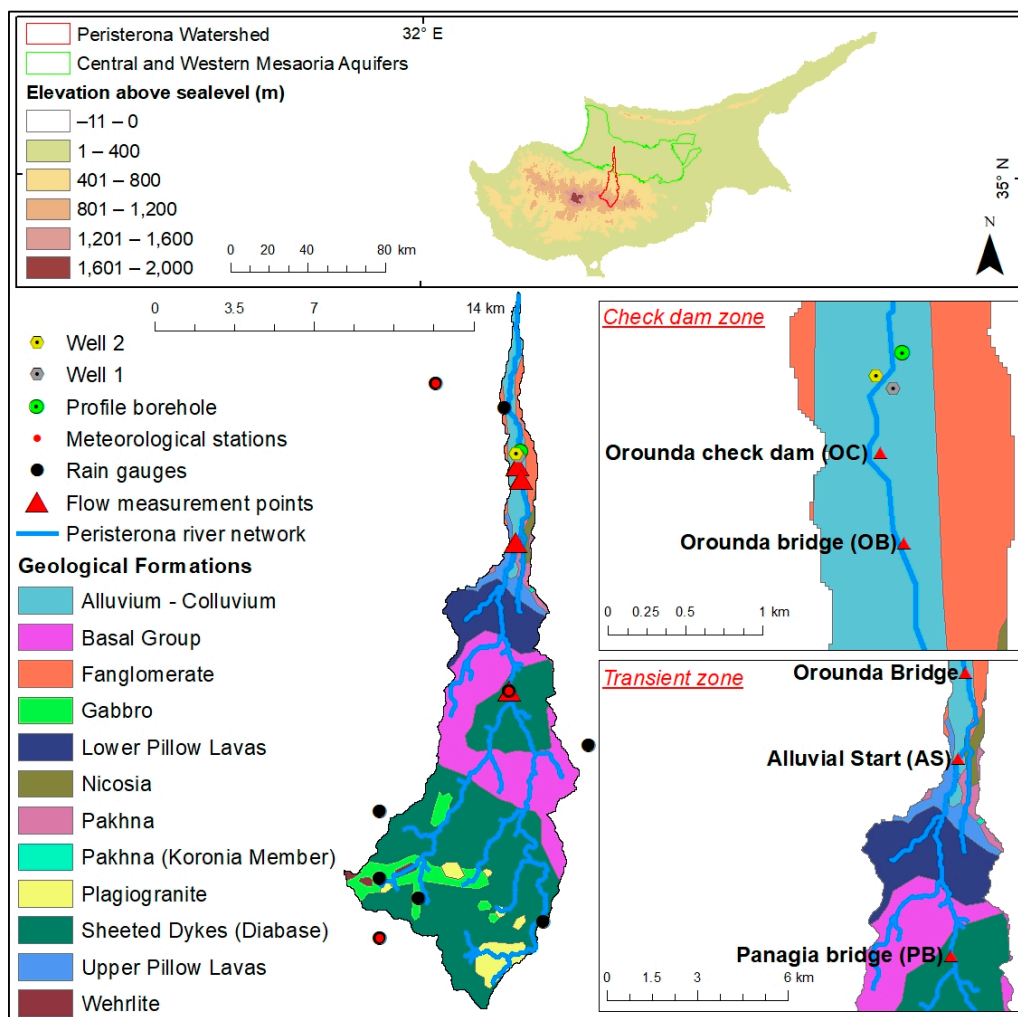


Figure 1. Location of the Peristerona Watershed and the Central and Western Mesaoria Aquifers [26] in Cyprus and its geology with the transient and check dam zones magnified and the streamflow measurement locations marked (modified from the Digital Elevation Model and Geological Map of Cyprus, Cyprus Geological Survey Department).

The study transect can be divided into two zones (Figure 1): the transient zone and the check dam zone. The transient zone is where water flows without ponding, while the check dam zone is where the inflowing water flow ponds and flows out of the check dam reservoir. Seven groundwater recharge check dams have been constructed along the Peristerona River on sedimentary formations in the Mesaoria plain. The most upstream check dam (named Orounda check dam) was selected for this research (Figure 1). This structure was completed in October 2011, while the other six were constructed between 1980 and 1990 (not shown).

2.1.1. Transient Zone

The river segment from Panagia Bridge (PB) to Orounda Bridge (OB) is 11 km long and is referred to as the transient zone in this study (Figure 1). The geology of the transient zone can be divided into two sections: the first section is located between PB and Alluvial Start (AS), with a length of 7.8 km, and its bedrock is composed of intrusive and volcanic rocks. The second section is located between AS and OB, with a length of 3.2 km, and its bedrock consists of alluvium and colluvium. The watershed area up to PB is 77 km², up to AS 98 km², and up to OB 105 km².

2.1.2. Check Dam Zone

Orounda Bridge (OB) is the entrance of the check dam zone, and the Orounda check dam spillway (OC) is the exit. This structure is made of gabions. The check dam, with its reservoir (a) and a cross-section of the check dam (b), is presented in Figure 2. The check dam wall has five concrete pipes with 0.5 m diameters. The elevation of the inlet of the pipes varies up to 10 cm, and the slope ranges between -0.6% and 0.3% . The spillway is constructed on top of the pipes and is 30 m long (the pipe spacing is about 6 m), 9.5 m wide, and 1 m high. The check dam is constructed on an alluvial riverbed, characterized by coarse gravel, cobbles, and few boulders. A nearby profile borehole (see Figure 1 for location) shows that the aquifer consist of boulders and gravel to a depth of 6 m, silty sand with fine gravel from 6 to 18 m, fine gravel with sandy marl from 18 to 21 m, sand from 21 to 52 m, and marl from 51 to 334 m (Cyprus Geological Survey Department).

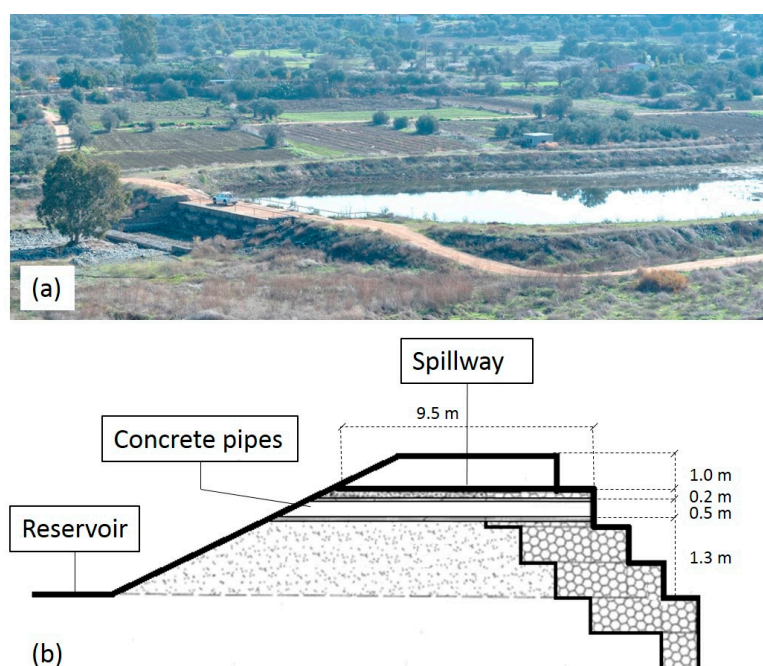


Figure 2. Orounda check dam with (a) its reservoir and (b) its cross-section.

2.2. Field Monitoring

The Water Development Department of Cyprus has measured streamflow continuously at PB with a weir since 1960. In addition to the continuous measurements, instantaneous streamflow measurements were made twice per week. The streamflow velocity was measured with an electromagnetic flowmeter (OTT MF pro; Kempton, Germany) at 0.6 of the depth and multiplied by the cross-sectional area of the stream water profile to obtain discharge ($\text{m}^3 \text{s}^{-1}$) using the mid-section method [27]. The distances between the stations (vertical sections) in each profile were such that no individual station contains more than 10% of the total discharge. The maximum observed streamwater profile was 0.7 m deep and 11 m wide. Measurements were made during the 2014 to 2015 streamflow season (December 2014 to June 2015) at two locations (AS and OB). Between these points, two irrigation channels, one on the east bank and one on the west bank, divert some of the stream water to the downstream agricultural fields. Twice weekly measurements of flow in these channels were made to estimate the amount of water diverted. Diversions to the irrigation canals were irregular. Also, sometimes water was released back to the streambed downstream from the canal inlets and before OB.

For the check dam zone, flow measurements were made at OB and OC (Figure 1) approximately twice per week during 2014 to 2015. In addition, the groundwater levels in two wells were measured approximately twice per week. The well locations are presented in Figure 1. Detailed topographic

mapping (scale of 1:1000) of the check dam area was made, when the river had no water in Summer 2013. Differential Global Positioning System (DGPS) and a total station (Leica, Heerbrugg, Switzerland) were employed. A Triangular Irregular Network (TIN) model was created from the acquired points using ArcGIS (ESRI, Redlands, CA, USA). With known dimensions, relations between water inflow, depth of the water in the check dam reservoir (h), and open water surface area (A) were established.

The volume and mass of sediment in the ponding area were measured in Summer 2013 and 2015. The depth of the sediment layer was measured with utility poles. Bulk density samples (kg m^{-3}) of the sediment profile were collected and averaged to compute the sediment mass from 24 locations.

2.3. Water Balance Computations

For the transient zone, linear regression relations were derived to link the continuous flow measurements at PB to the instantaneous flow measurements at AS and OB. The obtained relations were then used to estimate the daily flow at AS and OB for the period from 2011/2012 to 2014/2015 (hydrological years). Hydrological years are considered from 1st September to 31st August. The difference in the total flow between the two measurement points was considered groundwater recharge (above zero) or discharge (below zero). An estimate of the evaporation from the transient zone was made with Equation (2) presented below, using data from nearby stations and multiplying it with the surface area of the stream water, estimated from satellite images.

To estimate the groundwater recharge from the check dam, water balance calculations, the main components of which are presented in Figure 3 and Equation (1), were made. The daily check dam recharge was calculated as:

$$Q_r = Q_{in} - Q_{out} - Q_e + V_d - V_{d-1} \quad (1)$$

where Q_r is the recharge from the reservoir area, Q_{in} is the water inflow, Q_{out} is the water outflow, Q_e is the evaporation, and V_d and V_{d-1} are the volumes of water stored in the check dam reservoir area on the current and previous day, respectively. All units are in m^3 .

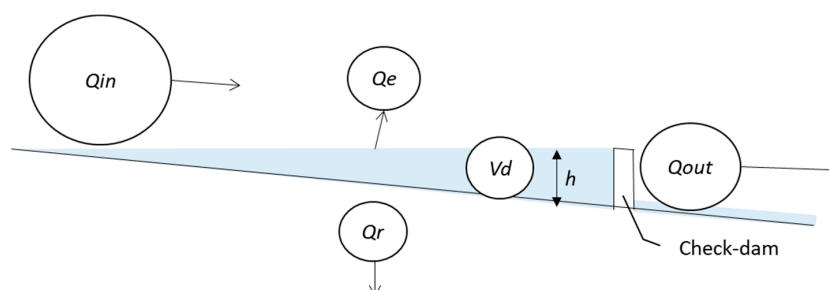


Figure 3. Check dam water balance components.

The inflow (Q_{in}) was estimated with a linear regression model. Evaporation was calculated using an equation that is a combination of the mass-transfer equation introduced by Harbeck [28] (suitable for lakes with a surface area (A) in the range of $50 \text{ m} < A^{0.5} < 100 \text{ km}$ located in arid environments) and the equation of Penman and Priestley-Taylor modified by de Bruin [29]:

$$Q_e = \left(\frac{\alpha}{\alpha - 1} \right) \left(\frac{\gamma}{\Delta + \gamma} \right) f(u) (e_s - e) A \quad (2)$$

where A is the area of surface water (m^2), γ is the psychrometric coefficient (-), e_s is the mean saturation vapour pressure of the air (kPa), e is the actual vapour pressure of the air (kPa), Δ is the slope of the vapour pressure curve (kPa C^{-1}), and α is the Priestley-Taylor coefficient defined as:

$$\alpha = \frac{(1 + \frac{\gamma}{\Delta})}{(1 + \beta)} \quad (3)$$

where unitless β is the ratio of sensible to latent heat flux with a default value of 0.6 [30]. The value of the function of wind speed ($f(u)$) is derived from the mass-transfer equation introduced by Harbeck [28]:

$$f(u) = 2.909A^{-0.05}u \quad (4)$$

where u is a wind speed 2 m above ground (m s^{-1}). Daily meteorological data is obtained from nearby stations.

Actual measurements of flow at OB and OC and measurements of h (the water height in the check dam) were used to relate, through regression models, h to $V_d(h)$, $Q_{out}(h)$, and $Q_r(h)$. To derive $Q_r(h)$, water balance calculations were performed only with actual measurements. The derived functions were used to calculate the daily potential Q_{out} and Q_r , which set the daily upper limits. However, the actual Q_{out} and Q_r values can be lower than the estimated $Q_{out}(h)$ and $Q_r(h)$ because the rate of the change in h throughout a day is ignored. In order to average this change and reduce the error in the estimates, the h value in the middle of a day (h_{mid}) is taken for the calculations; h_{mid} is the h of the total water at the end of the previous day in the reservoir plus half of the Q_{in} of the current day. Summarizing, daily Q_r and Q_{out} were calculated as:

$$Q_r = \min\left(Q_r(h_{mid}), V_{d-1} + \left(\frac{Q_{in}}{2}\right) - Q_e(h_{mid})\right) \quad (5)$$

$$Q_{out} = \begin{cases} \min(Q_{out}(h_{mid}), V_{d-1} + Q_{in} - Q_r - Q_e(h_{mid}) - V_{p1}) & \text{for } V_d > V_{p1} \\ 0 & \text{for } V_d \leq V_{p1} \end{cases} \quad (6)$$

where $Q_e(h_{mid})$ is the volume of water evaporated from an open water reservoir area given a water height h_{mid} , and V_{p1} is the volume of the water (m^3) up to the bottom of the pipes.

Considering the amount of annual rainfall and the dimensions of the check dam and the spillway, it is assumed that when the water level reaches an elevation above the spillway bottom, all overflow is exhausted in a single day. Therefore, for V_d , Q_e , and Q_r calculations, h is limited up to the spillway bottom elevation. The calculations were performed with Microsoft Excel[®] (Redmond, WA, USA).

2.4. Uncertainty Analyses

Uncertainty is presented by calculating the 90% prediction intervals of the estimated values [31]. These prediction intervals are referred to as uncertainty intervals and are expected to cover measurement errors. Errors in the discharge measurement with an electromagnetic flowmeter are computed as $\pm 6\%$. This value is the average calculated from six stations (single depth acquisition) with a declared accuracy of the OTT flowmeter of 2% [27,32]. All measured streamflow values were less than $6 \text{ m}^3 \text{ s}^{-1}$. In the literature, comparable error values have been reported for similar measurement ranges [33]. For the weir measurements, errors are also assumed to be $\pm 6\%$ [34]. The uncertainty intervals of the evaporation estimates were considered $\pm 5\%$, based on literature [35].

The upper and lower bounds of the uncertainty intervals were calculated both for the transient flow and the check dam zone. In addition to the model results with the best estimates (BE) of the components, the water balance was recalculated with the upper and lower bound uncertainty interval values of each component. The aim was to obtain maximum recharge (Q_{r_max}) and minimum recharge (Q_{r_min}) estimates as follows:

$$Q_{r_max} = Q_{in_max} - Q_{out_min} - Q_{e_min} + V_d - V_{d+1} \quad (7)$$

$$Q_{r_min} = Q_{in_min} - Q_{out_max} - Q_{e_max} + V_d - V_{d+1} \quad (8)$$

where Q_{r_min} , Q_{in_min} , Q_{out_min} , and Q_{e_min} are the lower bounds and Q_{r_max} , Q_{in_max} , Q_{out_max} , and Q_{e_max} are the upper bounds of the uncertainty intervals. Negative lower bounds were set to zero.

3. Results and Discussion

3.1. Transient Zone

Figure 4 shows the linear regression fits of the observed flow discharge (2014 to 2015) at PB with AS (Figure 4a) and OB (Figure 4b). The linear relation models produced reliable results because the watershed area between PB and OB is relatively small compared with the total watershed area (27% of the total watershed area) and no secondary streams with continuous flow contribute to the river in between these points. Another reason for the calculated good fit is that the watershed area upstream of PB receives most of the precipitation (area-averaged precipitation is 1.7 times more than the precipitation between AS and OB) and would be expected to produce more runoff, as it is the mountainous region of the watershed. As expected, the uncertainties for the PB-AS stretch are slightly lower than those for the longer PB-OB stretch. Any computed negative values were assumed to be zero. The modelled flow at AS and OB was considered to be zero for the days when the measured flow at PB was zero. Our field observations supported this assumption.

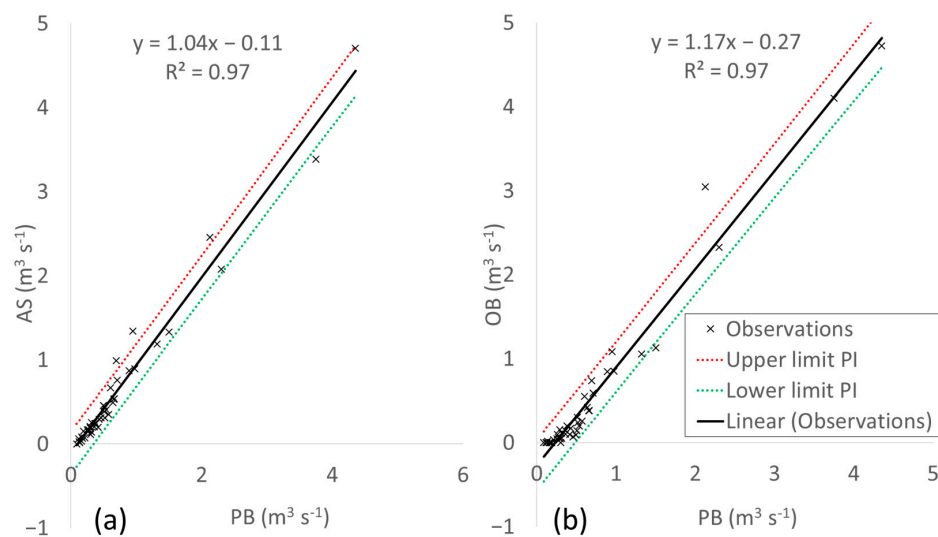


Figure 4. Linear regression of the observed flow data at Panagia Bridge weir (PB) with (a) Alluvial Start (AS) and (b) Orounda Bridge (OB), with 90% prediction intervals.

Based on these linear models, the flow at PB needs to exceed $0.10 m^3 s^{-1}$ to be hydraulically connected to AS and $0.23 m^3 s^{-1}$ to be connected to OB. This was expected since the distance between PB and OB is longer than that between PB and AS. In addition, when the discharge at PB is less than $2.5 m^3 s^{-1}$, the discharge at AS is lower than PB, indicating transmission losses from the stream (groundwater recharge) along the PB-AS river stretch. When the discharge at PB exceeds $2.5 m^3 s^{-1}$, the discharge at AS is greater than that at PB, indicating river discharge gains from groundwater or small side streams. Similarly, for the AS-OB river stretch, the threshold between transmission losses and gains can be set for a discharge at AS of $1.2 m^3 s^{-1}$. The Cyprus Geological Survey Department measures groundwater levels approximately once per month in wells in the proximity of the river bed. The groundwater surface elevation in these wells from 2011 to 2015 was never higher than the streambed elevation during the streamflow season, suggesting that the increase in streamflow downstream of AS is most likely caused by side streams. Similar streamflow behavior has been reported in the literature for rivers in arid and semi-arid climates, e.g., [36–38]. Barthel and Banzhaf [38] noted the difficulties of modelling such surface water and groundwater interactions because the parameters tend to exhibit large spatial and temporal variabilities.

3.2. Check Dam Zone

Figure 5a presents the relations between check dam storage volume, open water surface area, and water height, and Figure 5b presents the TIN model of the check dam topography created with the data collected in Summer 2013. The volume of the check dam storage up to the bottom of the pipes (261.07 m a.s.l.) was calculated as 14,216 m³, and up to the spillway bottom (262 m a.s.l.) as 24,923 m³.

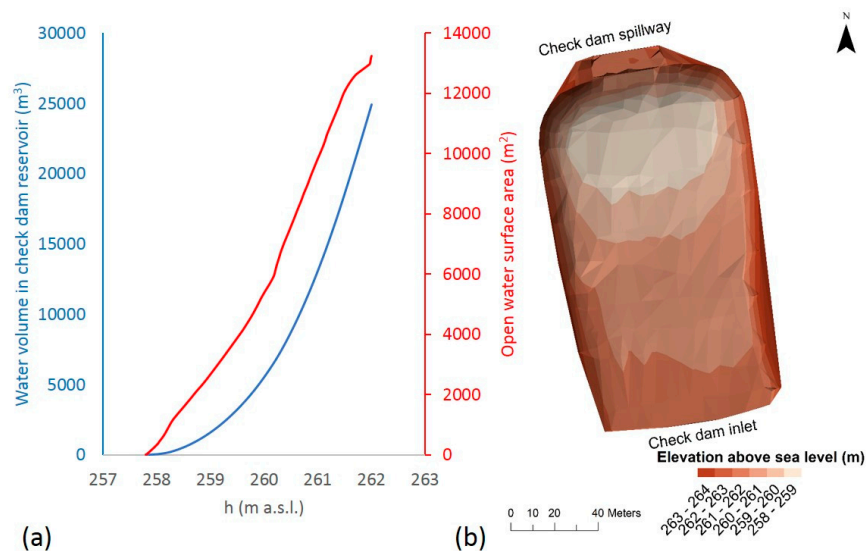


Figure 5. (a) Check dam storage volume (primary y -axis) and open water surface area (secondary y -axis) changes with water height; (b) TIN of the check dam created with topographic data collected in Summer 2013.

Figure 6a,b presents, respectively, the Q_r values obtained by water balance calculations with observed data and their exponential relation to h and the observed values of Q_{out} and h and a third order polynomial trendline, which was used for modelling the potential daily $Q_{out}(h)$ up to the spillway bottom. The upper and lower limit lines of the 90% prediction interval are also presented.

The derived exponential Q_r - h relation is supported by the exponential increase of the water volume in the check dam reservoir with increasing h (Figure 5a). This equation was used to model the potential $Q_r(h)$. It can be seen from the Q_r - h observations that Q_r increases slowly with increasing h and then (around h equal to 3.8 m) increases abruptly. This can be caused by the fact that the bottom of the check dam reservoir is below the ground level of the surroundings and the lower part of the reservoir walls are thicker than the upper parts and partly covered with sediment. The upper parts of the reservoir walls are above ground level, built with boulders and without sediment cover. Therefore, Q_r can occur slowly to a certain level of h and then increase rapidly. However, instead of having two Q_r - h relations (one for smaller and one for higher values than the threshold h), a single exponential relation was assumed. The single exponential relation has the advantage of reflecting, better than two distinct linear relations, the expected uncertainties associated with the Q_r estimates, as the upper and lower limits of the prediction interval show a relatively wide possible range of Q_r values given a certain h . High uncertainties are expected because of three main reasons: (i) the hourly change in Q_r is expected to play a role and daily measurements alone are not able to reflect this; (ii) Q_r is calculated from measured water balance components, which means that the measurement errors of each component contribute to the error in Q_r estimates; and (iii) sediment build-up in the reservoir can cause changes in Q_r over time. Frequent measurements of the flows and sediment-build up could improve the Q_r estimates.

Figure 6b shows that, although the observed pipe discharge (Q_{out}) is affected by differences among the bottom heights and slopes of the pipes and by disturbances at the inlet of the pipes, the Q_{out} - h polynomial relation is similar to the typical water depth to discharge relation for circular pipes.

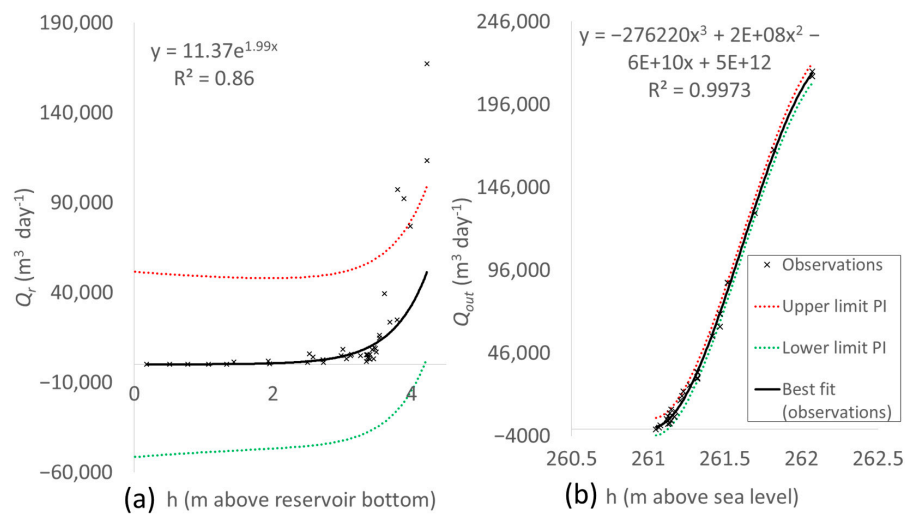


Figure 6. (a) Groundwater recharge (Q_r) values (derived from water balance calculations with observed data) and (b) observed check dam outflow (Q_{out}) with reservoir water depth (h) and best-fit trend lines with upper and lower limit of 90% prediction interval.

3.3. Water Balance Components

Table 1 shows the total annual water balance components of the transient and the check dam zones. From the 11 km long transient zone, a total of 5.96 million m^3 stream water is lost as transmission losses or recharged to the groundwater over four years. Evaporation is calculated to be 8% of the total loss (not presented). For this zone, the total losses are 4.6 times higher for the segment between PB and AS (7.8 km long on fractured bedrock) than for the segment between AS and OB (3.2 km long on alluvial deposits). This could be due to three main reasons: (i) the majority of the flow is generated upstream of PB, and, because PB-AS and AS-OB are both segments with transmission losses, the downstream stretch (AS-OB) receives less flow for recharge (over the four year period, there were 1029 days of flow at PB, 605 days at AS, and 401 days at OB); (ii) the PB-AS segment crosses four different geological units (Figure 1), two of which are classified as high-groundwater-recharge units due to their fractured nature [21], so preferential flow paths potentially exist and transmission losses and groundwater recharge could be higher than in the alluvial deposits [38,39]; and (iii) a faster increase of the streamflow at AS-OB compared with PB-AS. Several field observations support the third reason as the most important. The PB-AS segment is mostly covered with natural vegetation (e.g., coniferous forest), which creates surface runoff with relatively higher rainfall events in comparison with the bare land for the segment AS-OB [18]. In fact, opposite to AS-OB, the streams at PB-AS were observed to start flowing and discharging only after high rainfall events. In addition, irrigation diversions along AS-OB can also be reasons for a rapid increase of the streamflow. The capacity of the irrigation canals is limited and, after large flows, their inlet can be blocked by the debris. The effect of the third reason can be observed when we compare the model estimates of the streamflow of a wet and a dry year. During the wet 2011 to 2012 season, the model estimated a total 0.7 million m^3 increase in streamflow between AS and OB, while, during the dry 2012 to 2013 season, along the same stretch, the model estimated a total of 1 million m^3 in transmission losses.

Table 1. Observed flows at Panagia Bridge (PB) and modelled flows at Alluvial Start (AS) and Orounda Bridge (OB), constituting the water balance components of the transient and check-dam zone, where Q_r is the recharge from the reservoir area, Q_{in} is the water inflow, Q_{out} is the water outflow, and Q_e is the evaporation with the best estimate. The uncertainty intervals of the modelled results are presented.

Year	Precip. ^a (10 ⁶ m ³)	Transient Zone					Check Dam Zone					
		Flow at PB (Observed) (10 ⁶ m ³)	Flow at AS (Modelled)		Flow at OB = Q_{in} (Modelled) (10 ⁶ m ³)		Q_r (10 ⁶ m ³)		Q_e (10 ⁶ m ³)		Q_{out} (10 ⁶ m ³)	
			B ^b	L-U ^b	B	L-U	B	L-U	B	L-U	B	L-U
		2011–2012	75.56	23.99	23.13	19.56–28.74	23.84	20.24–30.43	5.86	0.26–13.04	0.007	0.014–0.014
2012–2013	52.38	8.61	7.22	4.46–12.65	6.25	3.97–12.62	2.93	0.04–8.56	0.004	0.014–0.013	3.31	4.05–3.92
2013–2014	37.95	1.63	0.41	0.01–6.26	0.04	0.00–6.90	0.04	0.00–6.87	0.001	0.004–0.017	0.00	0.01–0.00
2014–2015	65.54	13.39	11.95	8.99–18.09	11.54	8.91–18.74	3.62	0.07–10.14	0.004	0.008–0.013	7.91	8.57–8.83
Total	231.43	47.62	42.72	33.03–65.73	41.66	33.13–68.69	12.44	0.37–38.61	0.02	0.004–0.06	29.21	30.00–32.71

Notes: ^a Precipitation is calculated over the watershed area up to the check dam with area-weighted average, based on Thiessen polygons created with eight rain gauges. ^b B: Best estimate, L-U: Lower and Upper limit of the uncertainty interval.

For the check dam zone, 30% of the total four year inflow in the reservoir area was transformed into groundwater recharge (Table 1). The percentage of the recharge over the total inflow depends on the distribution of the inflow. The total amount of groundwater recharge in 2011 to 2012 was double the amount in 2012 to 2013. However, the percentage of the recharge over the total inflow for 2011 to 2012 was 25% and for 2012 to 2013 was 47%.

Our best recharge estimate from the check dam (30% of the streamflow) falls in between the ranges estimated by Martin-Rosales et al. [7] for 67 check dams in semi-arid south-eastern Spain. These authors simulated streamflow with a hydrological model and extrapolated recharge volumes from infiltrometer tests, performed on a permeable substrate similar to the one in our check dam area. The check dam reservoir volumes were also comparable: between 12,000 and 34,000 m³ for their study; 25,000 m³ in our research. They concluded that the percentage of recharge over the total inflow ranged between 6 and 53%, with higher values for higher check-dam capacities.

At the Panagia Bridge weir station (PB) (Figure 1), surface runoff from the up- and midstream areas averaged 16% of the precipitation during the drier years and 32% during the wetter years [40]. Based on our model estimates, the average annual recharge from both transient and check dam zones equals 4.6 million m³, which is 38% of the observed PB discharge. Based on groundwater model calibrations for the Western Mesaoria, Udluft et al. [41] found that groundwater recharge from rivers totalled 33.8 million m³ year⁻¹. Assuming that approximately one third of this amount is discharged by the Peristerona River, based on its watershed size relative to the other rivers, this number seems to overestimate recharge, considering that the mean annual discharge (1980 to 2010) of the Peristerona River at the Panagia Bridge weir station (PB, Figure 1) equals 9.75 million m³ year⁻¹ [40].

Figure 7 shows groundwater levels in Wells 1 and 2, the water level in the check dam, and the precipitation and inflow to the reservoir area over time. No groundwater level observations were made before January 2015. It can be observed that the groundwater levels follow a similar trend as the water levels in the check dam, while they do not relate to streamflow and precipitation, which can be considered an indication of active recharge from the check dam.

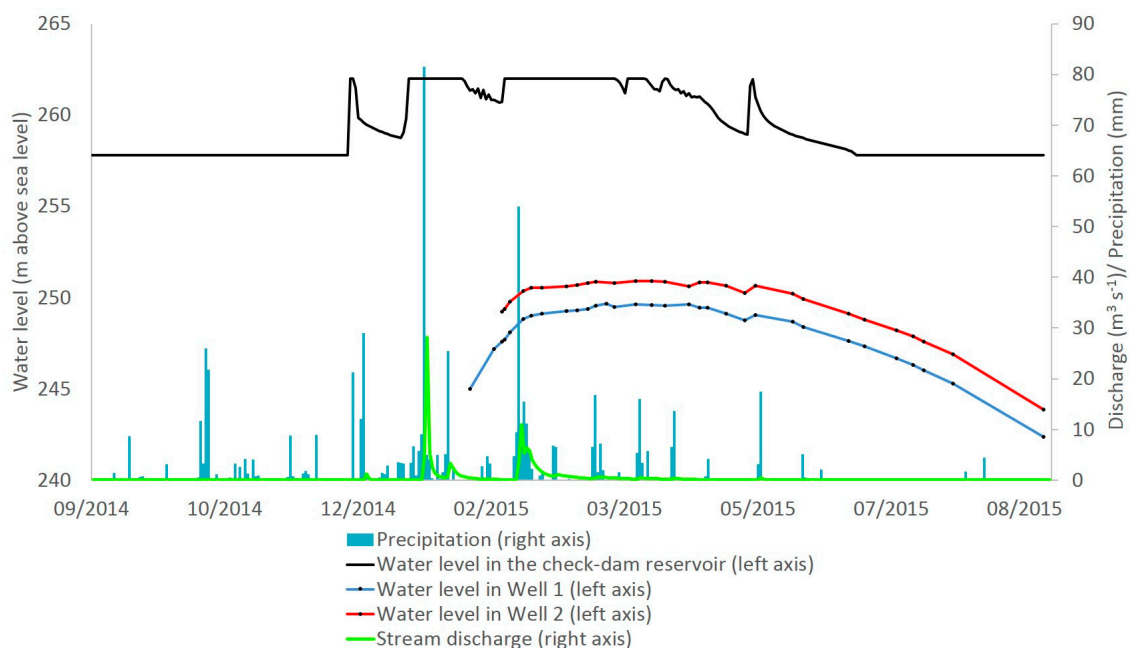


Figure 7. Water level in the check dam reservoir, water levels in the groundwater Wells 1 and 2, check dam inflow (stream discharge), and precipitation during the 2014 to 2015 season.

The uncertainty interval of the calculated Q_r (0.37 million m³ to 36.61 million m³) seems quite large (Table 1). However, it should be noted that running the model with upper and lower limits

(Equations (7) and (8)) is a maximalist interpretation of the errors. This approach assumes that all the water balance components are either at their upper or lower limits, which means that all errors in outflow, inflow, and evaporation affect simultaneously, at their maximum, the change in storage and are therefore reflected in the computed recharge. Nevertheless, it is remarkable to see such a great effect of the accumulated errors on the recharge for a water balance calculation.

3.4. Sediment Build-up in the Check Dam Reservoir

The average dry bulk density of the samples collected in 2013 was 1.1 g cm^{-3} (minimum: 0.9 g cm^{-3} , maximum: 1.2 g cm^{-3} , standard deviation: 0.1 g cm^{-3}) and, for the samples collected in 2015, was 1.1 g cm^{-3} (minimum: 0.8 g cm^{-3} , maximum: 1.4 g cm^{-3} , standard deviation: 0.1 g cm^{-3}). There was no significant variation in the bulk density values between the samples collected from different depths and in different years. However, the surface samples from the two locations closest to the check dam inlet had slightly higher bulk density values ($1.2\text{--}1.4 \text{ g cm}^{-3}$) than the average for both years. This is because these samples were sandier than the others. This can be due to the fact that coarser sediments are deposited earlier than finer sediments when the water flow velocity is reduced by the check dam [42]. The average depth of the sediment at the sample locations in 2013 was 21.6 cm (maximum: 35 cm, minimum: 5 cm and standard deviation: 8 cm) and, in 2015, was 22 cm (maximum: 48 cm, minimum: 5 cm, standard deviation: 10.8 cm).

From the bulk density measurements (average 1.1 g cm^{-3}) and the elevation differences (average 21.6 cm between 2011 and 2013 and 22 cm between 2013 and 2015), the total sediment build-up in the check dam reservoir was estimated to be 2640 tons for the years 2011 to 2012 and 2012 to 2013 and 2770 tons for the years 2013 to 2014 and 2014 to 2015, showing no significant difference. However, the total modelled streamflow into the reservoir was three times more for the former (Table 1). The season from 2011 to 2012 had above-average inflow to the reservoir, and the 2013 to 2014 season had almost no inflow. Figure 8 shows the discharge into the reservoir per day and cumulative frequency of each day over the two-year periods of 2011 to 2013 and 2013 to 2015. It can be seen from Figure 8 that the years 2011 to 2013 had more days with higher discharge compared with the years 2013 to 2015. The years 2011 to 2013 had ten days with high flow (occurring less than 4% of the time) and none above $1.5 \text{ million m}^3 \text{ day}^{-1}$, and the years 2013 to 2015 had only five days with high flow, one of which was an extreme event ($2.4 \text{ million m}^3 \text{ day}^{-1}$ on 6 January 2015). These results indicate that the high flow events, occurring less than 4% of the time in our case, can carry and build up most, if not all, of the sediment. Visual assessment of the high-flow events also supports this deduction as the turbidity of the stream water for these events was significantly higher. Moreover, events occurring less than 4% of the time constituted 30% of the total inflow in 2011 to 2013 and 40% in 2013 to 2015. The importance of high-flow events for sediment transport, along Mediterranean rivers comparable to Peristerona, has been reported by many authors [43–46]. Rovira and Batalla [44] studied the temporal distribution of suspended sediment transport in a Mediterranean basin in north-eastern Spain and concluded that 90% of the total sediment flow was carried by flood events, which occur 30% of the time. Vericat and Batalla [45] reported, for a watershed in southern Pyrenees, that 74% of the total sediment load was carried by flood events that occur 4% of the time. Achite and Ouillon [46] investigated sediment transport in a mountainous watershed in Algeria for 40 years and concluded that most of the sediment was carried by the 10 to 15 highest daily discharges over a year.

Djuma et al. [18] computed the area-specific sediment yield for 2011 to 2013 as $1 \text{ tons hectare}^{-1} \text{ year}^{-1}$ for the Peristerona watershed, assuming a 15% sediment trapping efficiency of the check dam. This efficiency was based on the ratio of the watershed area (km^2) and the capacity of the check dam (m^3) [47] and ignores the amount of inflowing water. Assuming that the suspended sediment concentration in the water outflow is the same as that of the inflow, the trapping efficiency can be estimated to be around 30%, as the total water outflow from the check dam was 70% of the total water inflow (Table 1). Conversely, assuming that all the sediment is carried by extreme events (upper 4%)

then the trapping efficiency can be estimated to be around 6%, as the total outflow from the check dam was 94% of the total water inflow for these events.

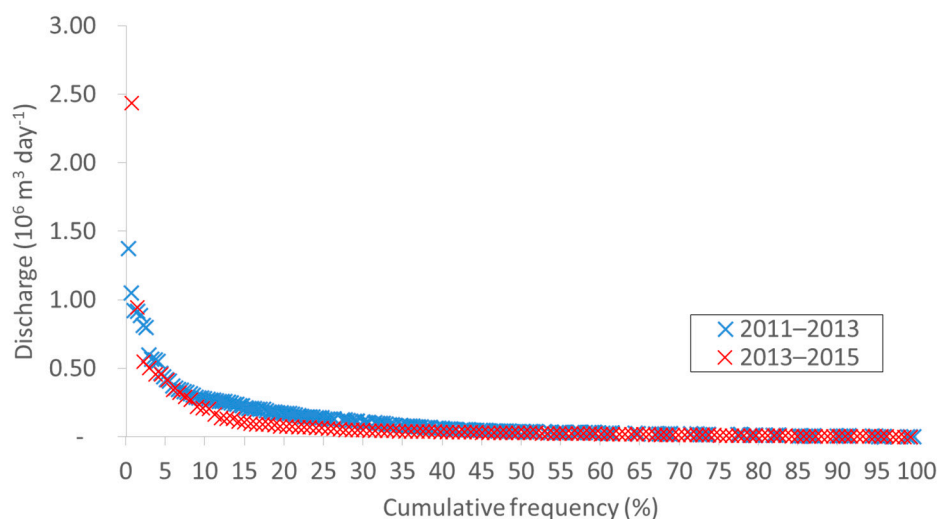


Figure 8. Discharge into the reservoir per day and cumulative frequency of each day over a two-year period for 2011 to 2013 and 2013 to 2015.

4. Conclusions

We found that a check dam with a reservoir capacity of around 25,000 m³ on an ephemeral river of a 105-km² watershed in Cyprus was able to recharge 2.1 times more groundwater than an 11-km-long river transect upstream of the check dam. This conclusion is an indication of the usefulness of such structures for the replenishment of groundwater resources in arid and semi-arid regions. We estimated the recharge through water balance calculations, and we stressed the high uncertainties of the results. This is mainly due to uncertainties in the inflow, which affect the change in storage and are reflected directly in the computed recharge. Continuous flow measurements can help to reduce the inflow uncertainties and better evaluate the performance of the check dam.

Our computations indicated that 70% of the water flowing into the check dam continued downstream. The distribution of the daily flow data indicated that the flow events occurring less than 4% of the time constitute more than 30% of the total check-dam inflow, and 94% of this inflow is discharged out of the check dam. Thus, due to the limited capacity of the check dam and the extreme discharge during these events, a large part of the potential groundwater recharge is missed. Further research is needed on the check dams downstream from the studied check dam (e.g., flow measurements and water balance calculations) to evaluate the usefulness of this series of structures.

To better evaluate the sedimentation rate and its effects on recharge, the check-dam sediment trapping efficiency should be evaluated per flow event with total water inflow, check-dam capacity, and turbidity sensors with continuous measurements, in addition to infiltration tests at the reservoir. The evaluation of sedimentation at the downstream check dams could also support these measurements. Erosion prevention techniques (e.g., afforestation, the revitalization or maintenance of abandoned agricultural dry-stone terraces, prevention of road erosion) can be applied at the watershed level to reduce the sedimentation in the check-dam reservoir area. These techniques have the added advantage of not only reducing soil erosion and keeping soil fertile but also increasing the groundwater recharge by limiting the sediment build-up.

Acknowledgments: We would like to thank our colleague Marina Faka for leading the topographic survey. We would also like to thank Christos Christofi from the Cyprus Geological Survey Department, Gerald Dörflinger from the Water Development Department, Filippos Tymvios from the Department of Meteorology, and their colleagues for providing data. This research received funding from the European Union Seventh Framework Programme (FP7/2007-2013) under grant agreement No. 603498 (RECARE project—Preventing and Remediating degradation of soils in Europe through Land Care).

Author Contributions: Hakan Djuma designed the methodology, collected and analysed the field data, and prepared the manuscript. Adriana Bruggeman and Corrado Camera supervised the study and helped with the field data collection and manuscript preparation. Marinos Eliades helped with the design and collection of the field data and reviewed the manuscript. Konstantinos Kostarelos provided advice on the methodology and helped with preparation of the manuscript.

Conflicts of Interest: The authors declare no conflicts of interest.

References

1. Chung, I.; Sophocleous, M.; Mitiku, D.; Kim, N. Estimating groundwater recharge in the humid and semi-arid African regions: Review. *Geosci. J.* **2016**, *20*, 731–744. [[CrossRef](#)]
2. Ringleb, J.; Sallwey, J.; Stefan, C. Assessment of managed aquifer recharge through modeling—A review. *Water* **2016**, *8*, 579. [[CrossRef](#)]
3. Steinel, A.; Schelkes, K.; Subah, A.; Himmelsbach, T. Spatial multi-criteria analysis for selecting potential sites for aquifer recharge via harvesting and infiltration of surface runoff in north Jordan. *Hydrogeol. J.* **2016**, *24*, 1753–1774. [[CrossRef](#)]
4. Guyennon, N.; Salerno, F.; Portoghese, I.; Romano, E. Climate change adaptation in a Mediterranean semi-arid catchment: Testing managed aquifer recharge and increased surface reservoir capacity. *Water* **2017**, *9*, 689. [[CrossRef](#)]
5. Rupérez-Moreno, C.; Pérez-Sánchez, J.; Senent-Aparicio, J.; Flores-Asenjo, P.; Paz-Aparicio, C. Cost-benefit analysis of the managed aquifer recharge system for irrigation under climate change conditions in Southern Spain. *Water* **2017**, *9*, 343. [[CrossRef](#)]
6. Martin-Rosales, W.; Gisbert, J.; Pulido-Bosch, A.; Vallejos, A.; Fernandez-Cortes, A. Estimating groundwater recharge induced by engineering systems in a semiarid area (southeastern Spain). *Environ. Geol.* **2007**, *52*, 985–995. [[CrossRef](#)]
7. Mussi, M.; Nanni, T.; Tazioli, A.; Vivalda, P.M. The Mt Conero limestone ridge: The contribution of stable isotopes to the identification of the recharge area of aquifers. *Ital. J. Geosci.* **2017**, *136*, 186–197. [[CrossRef](#)]
8. Alderwish, A.M. Induced recharge at new dam sites-Sana'a Basin, Yemen. *Arab. J. Geosci.* **2010**, *3*, 283–293. [[CrossRef](#)]
9. Racz, A.J.; Fisher, A.T.; Schmidt, C.M.; Lockwood, B.S.; Los Huertos, M. Spatial and temporal infiltration dynamics during managed aquifer recharge. *Ground Water* **2012**, *50*, 562–570. [[CrossRef](#)] [[PubMed](#)]
10. Huang, J.; Hinokidani, O.; Yasuda, H.; Ojha, C.S.P.; Kajikawa, Y.; Li, S. Effects of the check dam system on water redistribution in the Chinese Loess Plateau. *J. Hydrol. Eng.* **2013**, *18*, 929–940. [[CrossRef](#)]
11. Agarwal, R.; Garg, P.K.; Garg, R.D. Remote sensing and GIS based approach for identification of artificial recharge sites. *Water Resour. Manag.* **2013**, *27*, 2671–2689. [[CrossRef](#)]
12. Conesa-García, C.; García-Lorenzo, R. Bed scouring-sedimentation balance induced by check dams in semiarid catchments with different lithology. In *Check Dams, Morphological Adjustments and Erosion Control in Torrential Streams*; Conesa-García, C., Lenzi, M.A., Eds.; Nova Science Publisher: Hauppauge, NY, USA, 2013; pp. 283–306.
13. García-Lorenzo, R.; Conesa-García, C.; Martínez-Salvador, A. Assessing soil erosion in semi-arid check dam watersheds using GeoWEPP (South-East Spain). In *Geomorphology: Processes Taxonomy and Applications*; Miguel, H.S., Phillip, D.C., Eds.; Nova Science Publisher: Hauppauge, NY, USA, 2013; pp. 115–146.
14. Mandana, A.; Azlin, S.; Fauziah, A. Effectiveness of check dam to control soil erosion in a tropical catchment (The Ulu Kinta Basin). *Catena* **2012**, *97*, 63–70. [[CrossRef](#)]
15. Spalevic, V.; Lakicevic, M.; Radanovic, D.; Billi, P.; Barovic, G.; Vujacic, D.; Sestras, P.; Khaledi Darvishan, A. Ecological-Economic (Eco-Eco) Modelling in the River Basins of Mountainous Regions: Impact of Land Cover Changes on Sediment Yield in the Velicka Rijeka, Montenegro. *Not. Bot. Horti Agrobot. Cluj-Napoca* **2017**, *45*, 602–610. [[CrossRef](#)]

16. Tazioli, A. Evaluation of erosion in equipped basins: Preliminary results of a comparison between the Gavrilovic model and direct measurements of sediment transport. *Environ. Geol.* **2009**, *56*, 825–831. [[CrossRef](#)]
17. Rodriguez-Lloveras, X.; Bussi, G.; Francés, F.; Rodriguez-Caballero, E.; Solé-Benet, A.; Calle, M.; Benito, G. Patterns of runoff and sediment production in response to land-use changes in an ungauged Mediterranean catchment. *J. Hydrol.* **2015**, *531*, 1054–1066. [[CrossRef](#)]
18. Djuma, H.; Bruggeman, A.; Camera, C.; Zoumides, C. Combining qualitative and quantitative methods for soil erosion assessments: An application in a sloping Mediterranean watershed, Cyprus. *Land Degrad. Dev.* **2017**, *28*, 243–254. [[CrossRef](#)]
19. Camera, C.; Bruggeman, A.; Hadjinicolaou, P.; Michaelides, S.; Lange, M.A. Evaluation of a spatial rainfall generator for generating high resolution precipitation projections over orographically complex terrain. *Stoch. Environ. Res. Risk A* **2016**, *31*, 757–773. [[CrossRef](#)]
20. Boronina, A.; Renard, P.; Balderer, W.; Christodoulides, A. Groundwater resources in the Kouris catchment (Cyprus): Data analysis and numerical modelling. *J. Hydrol.* **2003**, *271*, 130–149. [[CrossRef](#)]
21. Mederer, J. Water Resources and Dynamics of the Troodos Igneous Aquifer-System, Cyprus—Balanced Groundwater Modelling. Ph.D. Thesis, Julius-Maximilians University of Würzburg, Würzburg, Germany, July 2009.
22. Zoumides, C.; Bruggeman, A.; Giannakis, E.; Camera, C.; Djuma, H.; Eliades, M.; Charalambous, K. Community-based rehabilitation of mountain terraces in Cyprus. *Land Degrad. Dev.* **2017**, *28*, 95–105. [[CrossRef](#)]
23. Cyprus Geological Survey Department. *Hydrogeological Map of Cyprus*; Cyprus Geological Survey Department: Nicosia, Cyprus, 1970.
24. United Nations Development Program. *Survey of Groundwater and Mineral Resources: Cyprus*; United Nations: New York, NY, USA, 1970; p. 231.
25. Karydas, C.G.; Tzoraki, O.; Panagos, P. A new spatiotemporal risk index for heavy metals: Application in Cyprus. *Water* **2015**, *7*, 4323–4342. [[CrossRef](#)]
26. Water Development Department. *Provision of Consultancy Services for the Implementation of Articles 11, 13 and 15 of the Water Framework Directive (2000/60/ec) in Cyprus—WDD 97/2007-Final Report on Water Policy, Annex VII*; Ministry of Agriculture, Natural Resources and Environment, Water Development Department: Athens, Greece, 2011.
27. OTT Electromagnetic Flowmeter Manual. Available online: <http://www.ott.com/en-us/products/download/ott-mf-pro-operating-instructions/> (accessed on 17 October 2017).
28. Harbeck, G.E. *A Practical Field Technique for Measuring Reservoir Evaporation Utilizing Mass-Transfer Theory*; USGS Professional Paper 272-E:101-105; US Geological Survey: Reston, VA, USA, 1962.
29. De Bruin, H.A.R. A simple model for shallow lake evaporation. *J. Appl. Meteorol.* **1978**, *17*, 1132–1134. [[CrossRef](#)]
30. Holtslag, A.A.M.; Van Ulden, A.P. A simple scheme for daytime estimates of the surface fluxes from routine weather data. *J. Clim. Appl. Meteorol.* **1983**, *22*, 517–529. [[CrossRef](#)]
31. Whitmore, G. Prediction limits for a univariate normal observation. *Am. Stat.* **1986**, *40*, 141–143.
32. ISO. *Measurement of Liquid Flow in Open Channels—Velocity-Area Methods*; Standard ISO 748; International Organization for Standardization (ISO): Geneva, Switzerland, 1997.
33. Tazioli, A. Experimental methods for river discharge measurements: Comparison among tracers and current meter. *Hydrol. Sci. J.* **2011**, *56*, 1314–1324. [[CrossRef](#)]
34. Boning, C.W. *Policy Statement on Stage Accuracy*; Technical Memorandum No. 93-07; USGS, Office of Water: Washington, DC, USA, 1992.
35. Stewart, R.B.; Rouse, W.R. A simple method for determining the evaporation from shallow lakes and ponds. *Water Resour. Res.* **1976**, *12*, 623–628. [[CrossRef](#)]
36. Ivkovic, K.M. A top-down approach to characterise aquifer-river interaction processes. *J. Hydrol.* **2009**, *365*, 145–155. [[CrossRef](#)]
37. Costa, A.C.; Bronstert, A.; De Araújo, J.C. A channel transmission losses model for different dryland rivers. *Hydrol. Earth Syst. Sci.* **2012**, *16*, 1111–1135. [[CrossRef](#)]
38. Barthel, R.; Banzhaf, S. Groundwater and surface water interaction at the regional-scale—A review with focus on regional integrated models. *Water Resour. Manag.* **2016**, *30*, 1–32. [[CrossRef](#)]

39. Dahan, O.; Shani, Y.; Enzel, Y.; Yechieli, Y.; Yakirevich, A. Direct measurements of floodwater infiltration into shallow alluvial aquifers. *J. Hydrol.* **2007**, *344*, 157–170. [[CrossRef](#)]
40. Le Coz, M.; Bruggeman, A.; Camera, C.; Lange, M.A. Impact of precipitation variability on the performance of a rainfall–runoff model in Mediterranean mountain catchments. *Hydrol. Sci. J.* **2016**, *61*, 507–518. [[CrossRef](#)]
41. Udluft, P.; Dünkeloh, A.; Mederer, J. Task 8: Groundwater Modelling on Selected Areas. In *Re-Evaluation of Groundwater Resources of Cyprus for the Republic of Cyprus*; Ministry of Agriculture, Natural Resources and Environment Geological Survey Department: Nicosia, Cyprus, 2004. Available online: http://www.hydrogeologie-wuerzburg.de/projects/grc_extended_abstract.pdf (accessed on 22 October 2017).
42. Ali, M.; Sterk, G.; Seeger, M.; Boersema, M.; Peters, P. Effect of hydraulic parameters on sediment transport capacity in overland flow over erodible beds. *Hydrol. Earth Syst. Sci.* **2012**, *16*, 591–601. [[CrossRef](#)]
43. Rovira, A.; Batalla, R.; Sala, M. Fluvial sediment budget of a Mediterranean river: The lower Tordera (Catalan Coastal Ranges, NE Spain). *Catena* **2005**, *60*, 19–42. [[CrossRef](#)]
44. Rovira, A.; Batalla, R. Temporal distribution of suspended sediment transport in a Mediterranean basin: The Lower Tordera (NE SPAIN). *Geomorphology* **2006**, *79*, 58–71. [[CrossRef](#)]
45. Vericat, D.; Batalla, R. Sediment transport from continuous monitoring in a perennial Mediterranean stream. *Catena* **2010**, *82*, 77–86. [[CrossRef](#)]
46. Achite, M.; Ouillon, S. Recent changes in climate, hydrology and sediment load in the Wadi Abd, Algeria (1970–2010). *Hydrol. Earth Syst. Sci.* **2016**, *20*, 1355–1372. [[CrossRef](#)]
47. Verstraeten, G.; Poesen, J. Estimating trap efficiency of small reservoirs and ponds: Methods and implications for the assessment of sediment yield. *Prog. Phys. Geog.* **2000**, *24*, 219–251. [[CrossRef](#)]



© 2017 by the authors. Licensee MDPI, Basel, Switzerland. This article is an open access article distributed under the terms and conditions of the Creative Commons Attribution (CC BY) license (<http://creativecommons.org/licenses/by/4.0/>).